Article

# A Cyclic Ion Mobility – Mass Spectrometry System

Kevin Giles, Jakub Ujma, Jason Wildgoose, Steven D. Pringle, Keith Richardson, David Langridge, and Martin R. Green

*Anal. Chem.*, **Just Accepted Manuscript** • DOI: 10.1021/acs.analchem.9b01838 • Publication Date (Web): 29 May 2019

# A Cyclic Ion Mobility – Mass Spectrometry System

Kevin Giles*, Jakub Ujma, Jason Wildgoose, Steven Pringle, Keith Richardson, David Langridge and Martin Green

Waters Corporation, Stamford Avenue, Altrincham Road, Wilmslow SK9 4AX UK

**ABSTRACT:** Improvements in the performance and availability of commercial instrumentation have made ion mobility – mass spectrometry (IM-MS) an increasingly popular approach for the structural analysis of ionic species as well as for separation of complex mixtures. Here, a new research instrument is presented which enables complex experiments, extending the current scope of IM technology. The instrument is based on a Waters SYNAPT G2-S*i* IM-MS platform, with the IM separation region modified to accept a cyclic ion mobility (cIM) device. The cIM region consists of a 98 cm path length, closed-loop travelling wave (TW)-enabled IM separator positioned orthogonally to the main ion optical axis. A key part of this geometry and its flexibility is the interface between the ion optical axis and the cIM, where a planar array of electrodes provides control over the TW direction and subsequent ion motion. On either side of the array, there are ion guides used for injection, ejection, storage and activation of ions. In addition to single and multi-pass separations around the cIM, providing selectable mobility resolution, the instrument design and control software enable a range of 'multi-function' experiments such as: mobility selection, activation, storage, $IMS^n$ and importantly, custom combinations of these functions. Here the design and performance of the cIM-MS instrument is highlighted, with mobility resolving power around 750 demonstrated for 100 passes around the cIM device using an inverse sequence peptide pair. The multi-function capabilities are demonstrated through analysis of three isomeric pentasaccharide species and the small protein ubiquitin.

Ion mobility spectrometry (IMS) is a rapid, gas-phase, separation technique which has been around for a significant number of years and has found particular utility as low cost, stand-alone portable detection devices for explosives and drugs of abuse.[1] In classical IMS experiments, packets of analyte ions travel through a gas-filled 'drift tube' under the influence of a uniform electric field and their arrival time at a detector recorded. The relationship between the drift velocity of ionic species and the strength of the applied electric field is governed by the mobility (K) of the ion in a buffer or drift gas. K is influenced by the instrument operational parameters of gas temperature and pressure, but more importantly for separation, the physico-chemical properties of the ion and the gas, including ion charge state, the ion and gas molecule masses and the rotationally-averaged collision cross-section (CCS) of the ion in the gas.[2] Whilst stand-alone IMS has a number of uses, the hybridization of IM with mass spectrometry (IM-MS) creates a significantly more powerful analytical tool, enhancing complex mixture analysis and facilitating ion structural determination through elucidation of CCS values.[3] IM-MS measurements find particular utility in analysis of isomeric ions, where different structural arrangements are reflected by differences in CCS. Furthermore, IMS offers significantly shorter separation timescales than liquid chromatography (LC) or gas chromatography (GC) such that these techniques can be combined with IM-MS measurements, offering three dimensions of selectivity/information. A benefit of introducing IM separation is its potential to reduce the need for long LC or GC separations prior to MS analysis, reducing overall analysis time and increasing throughput.

Developments in IM-MS technology and applications have experienced a rapid expansion over the last 30 years or so.[3,4] In the 1990s/early 2000s, the groups of Bowers, Jarrold, Clemmer and Hill, constructed custom IM-MS instrumentation and applied them to structural, biomolecular and complex mixture analysis.[5–12] Along with these foundational developments, further technological breakthroughs in sub-ambient pressure IMS have occurred. Perhaps the most important has been the use of electrodynamic ion confinement,[13] offering vast improvements in ion transmission through enhanced duty cycle and mitigating diffusion losses during separation.[14–19] As a consequence, IM-MS became an attractive proposition for mainstream analytical challenges, culminating in the release of a high performance commercial instrument by Waters Corporation in 2006, the SYNAPT HDMS.[20,21] This instrument had a quadrupole/IM/time-of-flight (ToF) MS geometry and utilized a new type of mobility separation based on travelling waves (TWs).[16] Thanks to technological developments, availability of commercial instrumentation[22,23] and developments in data analysis, IM-MS has become widely applied in fields of analysis ranging from petroleomics to structural biology.[24–29]

As with any analytical technology, there is constant drive to enhance and expand on the capabilities of IM-MS. As the IM-MS field develops, there is a focus from academia, industry and government sectors to improve the precision and reproducibility of IM measurements.[30–32] Much of the more recent technological progress has focused on the development of higher resolution IM separation capability. The diffusion limited resolving power ($R$) of both classical drift tubes and TWIM separators has been shown to depend on path length ($L$), applied electric field ($E$), charge of the ion ($Q$) and temperature of the buffer gas ($T$), via the relationship:[33,34]

$$R \sim \left(\frac{LEQ}{T}\right)^{1/2} \quad (1)$$

Thus there have been efforts to increase *R* via increasing path length,[35,36] electric field[37,38] and decreasing temperature.[39,40] Some novel concepts have been developed for increasing IM separation path length without significant increase in instrument footprint. Notably, a multi-pass cyclotron IMS was developed by Merenbloom *et al*.[41] There, the electric field is applied sequentially to four curved drift tube segments and ions with mobilities resonant with the field switching frequency are isolated within the cyclotron device. An IM spectrum is obtained by scanning the field switching frequency. *R* in excess of 1000 has been demonstrated with this approach.[42] TWIM technology offers a unique advantage in constructing long path and multi-pass IM separators. Unlike classical drift tubes, increasing the length of the TWIM device does not require concomitant increase in applied field or 'drift' voltage (≡ TW amplitude). Therefore, there are no practical issues, such as voltage breakdown or safety concerns when constructing long path length devices. Also, since the electrical potential at the start and end of a TWIM device is the same,[16] they are ideally suited for closed-loop, multi-pass separators. With this in mind, a compact, cyclic geometry, TWIM separator (cIM) was conceived.[43–45] Unlike the cyclotron device, ions of different mobility can simultaneously undertake many passes around the cIM geometry before being ejected out. The *R* of the cIM separator follows Equation 1, i.e. increasing as $\sqrt{n}$ ($\propto \sqrt{L}$) where *n* is the number of passes around the device. *R* therefore becomes a scalable, 'dial-up', instrument parameter and values up to 140 were shown for 6 passes.[44] The concept of long path length and multi-pass TWIM devices has also been explored by Smith and co-workers using their highly flexible structures for lossless ion manipulation (SLIM) technology,[46] where *R* values in excess of 1800 have been demonstrated for a separation path length of ~540 m.[47] Another novel approach to increase mobility resolution has been developed by Loboda where the use of opposing buffer gas flow was used to provide an effective increase in separation length in a compact geometry.[48] Using similar methodology but with ion pre-trapping using non-linear electric fields (trapped ion mobility spectrometry, TIMS), Park, Fernandez Lima and co-workers have demonstrated IM resolving power in excess of 400.[22,49–51]

Although an extremely desirable characteristic, the benefit of high mobility resolution alone can be limited when trying to solve more complex, real world problems. A parallel situation can be seen with MS technology where multiple stages of MS are successfully used to improve instrument capability, even with relatively low-resolution MS analysers. Tandem IMS instrumentation has been developed previously, notably by the Clemmer group,[19,52] and more recently by Li *et al.*,[53] and Liu *et al*.[54] A significant design feature of the cIM instrument reported here is that $IMS^n$ experiments can be performed,[55,56] as a parallel to $MS^n$, whereby mobility separated ions can undergo the sequence of selection, activation or fragmentation and re-separation any number of times before MS detection.

The design and performance of this quadrupole-cIM-ToF instrument is presented here, focusing both on mobility resolution and multi-function capability.

## INSTRUMENT DESIGN AND OPERATION

**Travelling Wave Ion Mobility.** The concepts behind travelling wave ion mobility (TWIM) have been described in detail elsewhere[16,33,57] and so will only be covered briefly here. Unlike classical drift tube systems, the TWIM utilizes a series of voltage pulses to propel ions through the buffer gas. As the 'waves' pass along the device, ions 'surf' on a wave front for a period of time before being overtaken by the wave. This process is repeated for the arrival of each subsequent wave. The frequency with which the ions are overtaken by the wave depends on their mobility. Ions of lower mobility get overtaken more frequently than those of higher mobility and so take longer to transit the device, giving rise to separation. A standard linear TWIM device comprises an RF-confining stacked ring ion guide (SRIG), with a 0.5 cm diameter aperture, and a continuous sequence of superimposed DC voltages travelling along the length.[16,58]

**The cIM Separator.** The cIM device and associated ion optics were installed in a modified SYNAPT G2-Si instrument, which has a quadrupole-TWIM-ToF geometry (Waters Corp., Wilmslow, UK). Figure 1A shows a schematic of the modified instrument, where the cIM is located orthogonally to the main ion optical axis, replacing the standard, 25.4 cm long co-linear TWIM device.[58] The cIM device comprises two active regions; the first is the main body of the separator (Figure 1B) and the second is the ion entry/exit region which intersects the main ion optical axis of the mass spectrometer (Figure 1B,C), which combined provide a 98 cm long mobility separation path length. The main body of the cIM device (Figure 1B) consists of 608 electrodes (0.05 cm thick, 0.15 cm centre-to-centre spacing) supported by printed circuit boards (PCB) which provide both the geometrical structure and the voltage connections. The electrode structure in the main separation region (Figure 1D), forms a 0.5 cm x 5 cm rectangular ion transmission channel. Opposite phases of RF voltage (up to 300 $V_{pk\text{-}pk}$ at 2.5 MHz) are supplied to adjacent plates in the y-direction to provide a pseudo-potential barrier and consequent ion confinement in the z-direction. Ions are confined in the x-direction by a DC voltage (60 V, just above the maximum TW amplitude) applied to the 'repeller band' electrodes formed by tracks on the PCB substrate material. The TWs (up to 45 V and velocities of 300-1000 m/s) are applied to the RF electrodes with a repeat pattern of four plate-pairs, with two plate pairs 'on' and two plate pairs 'off' and a propagation step of one plate pair[58] travelling in the y-direction. The described rectangular geometry has specific benefits for a closed-loop TWIM separator, compared with the standard 0.5 cm aperture ring electrodes used in linear TWIM devices: (i) It increases charge capacity. Larger ion currents are expected through increased separation time, mandating longer storage times prior to ion release to the cIM. The charge capacity of the rectangular transmission channel has been calculated to be ~10X higher than that of the 0.5 cm diameter aperture linear TWIM device, see Figure S2A. (ii) It minimises the need for higher applied TW voltages. In TWIM devices, the strength of the electric field experienced by the ion during separation depends on relaxation of the applied voltage towards the center of the device.[58] Using a rectangular geometry, rather than a larger circular one, reduces this effect, reducing the need for higher TW amplitudes to maintain separation performance. (iii) With the short axis in the radial (z-) direction of the cIM (Figure 1D), possible 'racetrack' effects due to ions circulating at different radii are minimized. In practice, the ions are confined by the RF in the radial, z-direction, to a relatively narrow band (Figure S3). (iv) The strength of the RF ion confinement generated is dependent on the adjacent plate-electrode separation distance (y-dimension). To allow use of the same RF voltage on the inner and outer 'ring' of electrodes, and to maintain effective confinement, the radial separation of

the 'rings' should be minimal, limiting increase in adjacent plate separation in the outer 'ring' due to the curvature of the ion guiding channel. (v) The use of a DC voltage to confine ions in the x-direction (Figs. 1D and S2B), rather than a closed-loop RF electrode, removes an edge effect where ions would experience a higher TW amplitude in the vicinity, resulting in mobility peak distortion (Figure S4D).

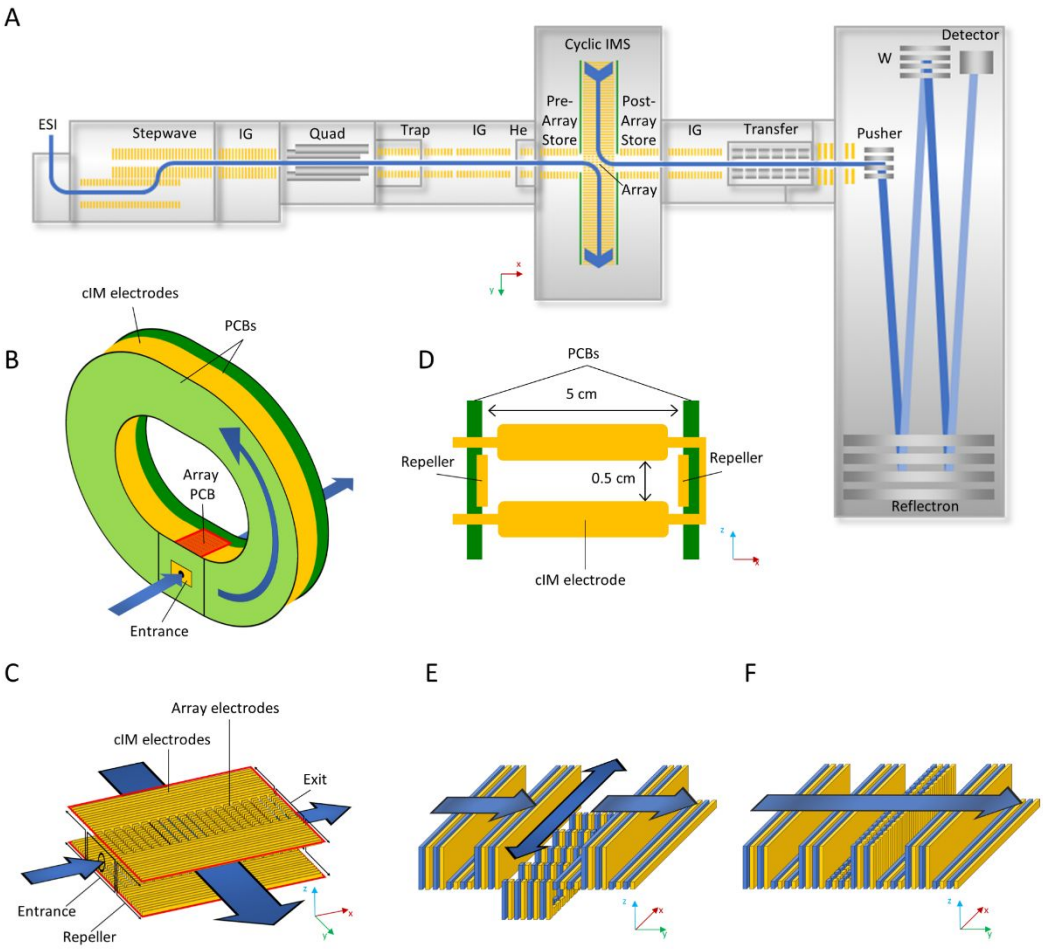


Figure 1. Instrument design. A: instrument overview (adapted in part with permission from ref 63. Copyright 2019, Ujma *et al.*) B: cIM device. C: ion entry/exit region, consisting of array electrodes. D: structure of cIM electrodes. E: Ion injection/ejection mode, array TWs are applied in the x-(or -x) direction. F: Separation mode, array TWs are applied in the y-direction.

To understand the implications of a closed-loop design on mobility resolution, comparison SIMION (v8.1, SIS Inc., Ringoes, NJ USA) simulations were made using various geometry arrangements, shown in Figures S1 and S3. These simulations indicate no significant detrimental effect of a closed-loop design on mobility resolution and show good agreement with experimental data (Figure S4E).

The second and key part of the cIM device is the ion entry/exit region (Figure 1C), which is designed to enable ion entry to the device, mobility separation and ion ejection without significant compromise in ion transmission or mobility resolution. To achieve this an array of electrodes was designed to allow TWs to operate in the entry/exit direction (x) for ion loading/ejection and in the orthogonal direction (y) for mobility separation (Figs 1E-F respectively). This region is constructed with the mounting PCBs orthogonal to those in the main section of the cIM for ease of construction (shown in red in Figure 1B, for photographs see Figure S5A-B). This geometrical orientation accounts for the 'racetrack' shape of the cIM device rather than a uniform circle (Figure 1B). On the PCBs there are 24 standard electrodes (as used in the main part of the cIM), 12 either side of the 8 array electrodes which are constructed from 0.05 cm thick edge plated PCBs (Figure S5B, inset). The entry into and exit from the electrode array is through 0.4 cm diameter apertures. These electrodes are plated on both sides of a PCB substrate, mimicking the repeller band electrode on the face adjacent to the array. In the separation (y) direction, the adjacent array electrodes have opposite phases of RF voltage applied (Figures 1E-F, depicted by yellow and blue colors); as described for the main cIM electrodes. In the ion entry/exit (x) direction, the array electrodes comprise five repeat sections of four elements (Figure S6). The operational modes of the TWs in the array shown in Figures 1E-F. During ion injection/ejection events (Figure 1E) the applied TWs are one array element wide and progress by stepping one array element at a time in the +x (or –x) direction. When undertaking mobility separation, the TWs are applied in the y-direction, in sequence with those in the main cIM (Figure 1E). The TWs in the main cIM are 'always on' while behavior of the array can be varied. Directly before and after the array region are SRIGs (Pre- and Post-array stores, Figure 1A) which are 4.4 cm long and comprise of 30 ring electrodes with 0.5 cm diameter apertures. These devices are located in the same chamber as the cIM and perform dual functions. Firstly, they are used to transport ions to and from the array region. Secondly, they can act as ion

storage regions, accepting mobility selected 'slices' of ions from the array (described in detail later). These SRIGs operate at an RF of 2.5 MHz and up to 350 $V_{pk-pk}$. Depending on the required operation, axial fields ranging from 0 to 10 V/cm are used to drive ions through these ion guides. Ion entry into the high pressure cIM chamber is through a helium cell, to reduce ion scattering and activation, as described elsewhere.[58] The helium cell has an 0.2 cm diameter entrance and exit aperture, as does the exit plate of the post-array store SRIG. The buffer gas ($N_2$) is supplied to the main body of the cyclic IM chamber, which is typically operated at a pressure of around 2 mbar. Pressure is measured using a capacitance diaphragm gauge (CDG025D, Inficon).

The pre-cIM chamber contains two SRIGs, the first is a standard Trap ion guide used in the SYNAPT G2-Si where ions are received from the quadrupole (resolving or non-resolving), accumulated whilst the previous mobility separation is occurring and then released as a packet, providing high duty cycle operation. Once released, the packet of ions pass through another, 15 cm long, SRIG device (IG, Figure 1A) comprising 101 electrodes with 0.5 cm apertures and an axial field which transports the ions to the He cell. The Trap is operated at a pressure of around $10^{-2}$ mbar of $N_2$ and the other SRIG at a background pressure of around $10^{-3}$ mbar, maintained by a 240 L/s turbo-molecular pump (nEXT240D, Edwards).

The post-cIM chamber also contains two ion guides, the first is a duplicate of the 15 cm long SRIG (IG) in the pre cIM chamber and the second, the Transfer ion guide, comprises a new segmented quadrupole with axial field. The axial fields are essential in these guides to maintain the fidelity of the mobility separation. The Transfer guide is operated at a pressure of around $10^{-2}$ mbar of $N_2$ and the SRIG at a background pressure around $10^{-3}$ mbar, maintained by a 240 L/s turbo-molecular pump (nEXT240D). Following the Transfer ion guide, ions pass to the ToF for mass analysis. Both the Trap and Transfer ion guides can operate as collision cells for fragmenting ions before and/or after mobility separation.

## *CYCLIC IM OPERATION*

The overall sequence for cIM analysis is to release the stored ions from the trap as a packet, transfer them to the cIM for separation/manipulation and finally eject and transport the mobility separated ions to the ToF mass analyser for detection and arrival time recording. The majority of the functionality required to achieve cIM separation is incorporated in the control of the array region. The potential energy diagram of the instrument region from the trap to the transfer device is shown schematically in Figure S7. The array has an independent bias and TW voltage setting with respect to the main cIM.

Descriptions of the basic cIM control, to provide the required functionality, are outlined below and illustrated in Figures 2 and S8.

**Injection:** The ion packet from the trap is transported to the array for holding, ready for the separation phase. During the injection phase (Figure S8A), the DC bias of the array electrodes is held below that of both the pre-array store and the main cIM electrodes. Holding it below that of the cIM creates a potential barrier to prevent ions entering the cIM separation region prematurely. A low-level TW (typically 2 to 5 V) is applied in the +x direction to help distribute ions throughout the 5 cm long array region (Figure 1E). The array exit aperture is held a potential above that of the array to prevent ions passing straight through to the post-array store. This state of the instrument is held until all ions have entered the array region. Injection times are typically in the range of 5 to 15 ms.

**Separation:** In this phase, the DC offset of the array electrodes is set to match that of the main cIM, shifting the potential of the confined ions (Figure S8B). The voltages applied to entrance and exit apertures are increased to match that of the repeller electrode, making the array region resemble the main cIM (Figure S8B). The direction and amplitude of the TWs applied to array electrodes are switched to match those in the main cIM (Figure 1F). Ions are then begin propelled around the cIM separator. For a single pass (base mobility resolution), separation times need to be sufficiently long for ions to exit the array but not too long that ions undertake more than one pass. Typically, for a single pass separation the device would be set to the potentials shown in Figure S8B for 2 to 5 ms. For multiple passes (higher mobility resolution), the time for this phase can be extended into the hundreds of ms range.

**Ejection:** *(i) to ToF*: After the required separation period, the DC offset of the array is lowered below that of the cIM but above that of the post-array store and the TWs switched to propel ions in the +x-direction towards the ToF analyser (Figures 1E and S8E). The main cIM TWs continue to operate, delivering mobility separated ions to the array. The offset of the exit aperture is reduced to facilitate ion transport out of the array. In this phase the TWs in the array region are set independently of the main cIM but need to be of sufficient amplitude and velocity to minimise any mobility peak broadening due to differences in ion transit time across the 5 cm length of the array (typical values are 25 V and 375 m/s). Upon exiting the array, the ions are transported through the post-array store, the IG and finally the transfer cell and into the ToF mass analyser. Typical times for the '*ejection-to-ToF*' function are in the tens of ms range, long enough for all ions to exit the cIM. Depending on the experimental sequence (discussed later), data acquisition can be triggered or not. In the latter case, the ions are transported to the ToF but not recorded. In this manner, ions are effectively disposed of. *(ii) to pre-array store*: The mobility separated ions can be also ejected into the pre-array store (Figure S8D). Again, the DC potential of the array is lowered below that of the cIM but above that of the pre-array store. The potential of the array entrance aperture is reduced to facilitate ion exit. The array TWs are applied in -x-direction (Figure 1E) and the axial electric field in the pre-array store is set zero. Thus, the mobility separated ions are delivered into the pre-array store.

**Bypass:** The orthogonal arrangement of the cIM also allows ions to be transported straight through the array, bypassing the main mobility section if standard, Q-ToF, operation of the mass spectrometer is required (Figures 2 and S8E). During this function, the potential of the array electrodes is set between those of the pre- and post-array store and operated with TWs in the +x-direction. In this mode there is no ion storage/release in the trap ion guide. DC potentials applied to both array entrance and exit are set to ensure continuous transmission.

## *MULTI-FUNCTION CAPABILITIES*

The basic control functions described above can be arranged in sequences, while timing and operating parameters can be adjusted on a 'per function' basis. A flexible, web-based, GUI has been developed to enable custom function sequences to be generated as part of the instrument control software (see Figure

S9). For example, a standard single or multi-pass IM separation would involve a sequence of *injection/separation/ejection-to-ToF*, where the duration of the separate function determines the number of passes the ions make around the cIM and hence the mobility resolution. Flexibility enabled by such sequential operation of the array region in the cIM allows some novel experiments to be performed.

**IMS$^n$:** During the separation phase of an experimental sequence the '*ejection to pre-array store*' function can be applied for a short amount of time (typically hundreds of µs), excising a segment of the mobility separated species (Figure S8D). The remainder of the ions in the cIM can be '*ejected-to-ToF*', without triggering data acquisition, to remove them. The stored ions can then be re-injected into the array under collision induced activation/dissociation conditions, as required, and subsequent mobility separation performed. The product ions can then be '*ejected-to-ToF*' for detection, with the acquisition sequence triggered, or can undergo a further mobility selection event and so on providing the IMS$^n$ capability. The re-injection of ions from the store to the array is a particular sequence function ('*inject-from-store*'), similar to '*injection*' (Figure S8A), but not linked with the release of ions from the Trap. The axial field in the store is re-applied to propel ions out. To activate the ions on re-entry to the array, the overall potential of the pre-array store is increased with respect to the array.

**IM Isolation:** This sequence can be used to reduce the mobility range of species in the cIM. It involves setting a sequence consisting of '*ejection-to-ToF/separation/ejection-to-ToF*' to eject ions (without acquisition) outside of the desired mobility range. Essentially, this leaves the remaining species in the cIM to continue the separation process and to some degree resembles the operation of the cyclotron IM device.[41] This 'trimming' approach can be undertaken a number of times and can be used, for example, to prevent 'wrap-around' in the cIM where high mobility ions catch up with low mobility ions in multi-pass experiments. Wrap-around is illustrated in Figure S10.

## *TOF-MS*

In comparison to the base SYNAPT G2-Si, the ToF analyser has been increased in length by around 40 cm, with the intermediate ('W') reflectron and detector being offset from the main instrument ion optical axis and the orthogonal acceleration 'pusher' (Figure 1A). This increased length, combined with improved ion beam conditioning using the segmented quadrupole Transfer cell enables *m/z* resolution of up to 100,000 to be realized (Figure S11).

## *DATA ACQUISITION AND INSTRUMENT CONTROL*

The analogue-to-digital converter (ADC) acquisition system used on this instrument is different from that on the standard SYNAPT G2-Si which utilizes a single 8-bit ADC and single amplification stage. In the Instrument described, two 10-bit ADC devices with independent signal amplification stages are utilized in tandem, providing up to 60X increase in dynamic range. This is valuable for mobility analyses due to the high ion currents encountered in the ms wide peaks. Also, there is an increase in available arrival time record length, from 200 to 250 'bins' (ToF mass spectra), to help accommodate the longer cIM separation time-scales. The data acquisition sequence is timed from a chosen time point, typically the instigation of the last '*ejection-to-ToF*' segment. Then a maximum of 250 sequential ToF mass spectra are acquired to record the ion arrival times.[10] Thus, the recorded arrival time distribution (ATD) would consist of a maximum of 250 bins. In a further enhancement, multiple ToF spectra can be 'binned' together to provide increased arrival time acquisition range albeit at a lower temporal resolution. As such, binning every two consecutive ToF mass spectra together results in doubling the time available

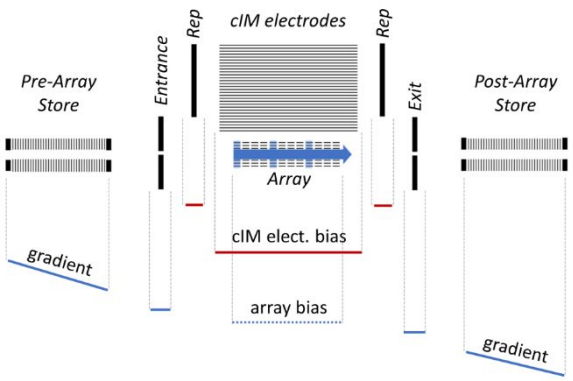


Figure 2. Potential energy schematic of the cIM region voltages during 'bypass' mode. Settings changeable on a 'per function' basis: blue lines. Settings changeable on 'per sequence' basis: red lines. Blue arrows indicate the array TW direction. Schematics of other functions are presented in the Figure S8.

in IM domain; and so on. Following the end of the 250-bin data acquisition, the cIM experiment sequence starts again with the ion packet release from the trap and the subsequent mass spectral data histogrammed with the previous. This loop continues for a chosen scan/acquisition period and then the data are transferred to a host PC. Then, the next scan period is started.

Instrument control and data acquisition are enabled through a custom designed web-based GUI (see Figure S9). Data are processed using MassLynx (v4.1) and a modified version of Driftscope (v2.9) (Waters Corp., Wilmslow UK).

## *MATERIALS AND METHODS*

Reverse sequence peptides, SDGRG and GRGDS were purchased from Cambridge Bioscience (Cambridge, UK). Ubiquitin (from bovine erythrocytes), acetonitrile (ACN), ammonium acetate and formic acid were purchased from Sigma-Aldrich (Dorset, UK). Three pentasaccharides: 1,4-β-D-Cellopentaose, Maltopentaose and α1-3,α1-3,α1-6 Mannopentaose were purchased from Dextra Laboratories Ltd (Reading, UK). The instrument was operated in positive ion mode ESI. The reverse peptides and three pentasaccharides were infused as mixtures in 50/50 Water/ACN/0.1% formic acid. Ubiquitin was infused at concentration of 1µM in 50 mM aqueous solution of ammonium acetate. The cIM was operated at 2 mbar of $N_2$ and the TWs at 375 m/s with amplitudes as stated in the relevant figures.

## RESULTS

**Resolution:** To evaluate the basic resolution characteristics of the cIM device, the inverse sequence pentapeptides SDGRG and GRGDS were infused as a mixture into the ESI source of the instrument. Figure 3 shows the separation of the $[M+H]^+$ ions (*m/z* 491.2, quadrupole-selected) as a function of the number of passes around the cIM device. It can be seen that the ionic species are partially resolved even with just one pass

around the cIM (98 cm) and, using the known *CCS* values,[45] a *R* of 78 (*CCS*/Δ*CCS*) is calculated, where Δ*CCS* is the extracted full width half maximum value of the mobility peak ATD. This value is close to the expected factor of two increase in mobility resolution over the 25.4 cm long linear TWIM cell of a standard SYNAPT instrument.[58] As the number of passes increase, *R* increases to a value of 350 after 16 passes (~15.7 m) where the peaks are well separated. Beyond 16 passes, the more mobile SDGRG starts to catch up with the GRGDS and consequently the separation is lost (wrap-around). To probe the resolution further, the '*IM isolation*' functionality, described above, was

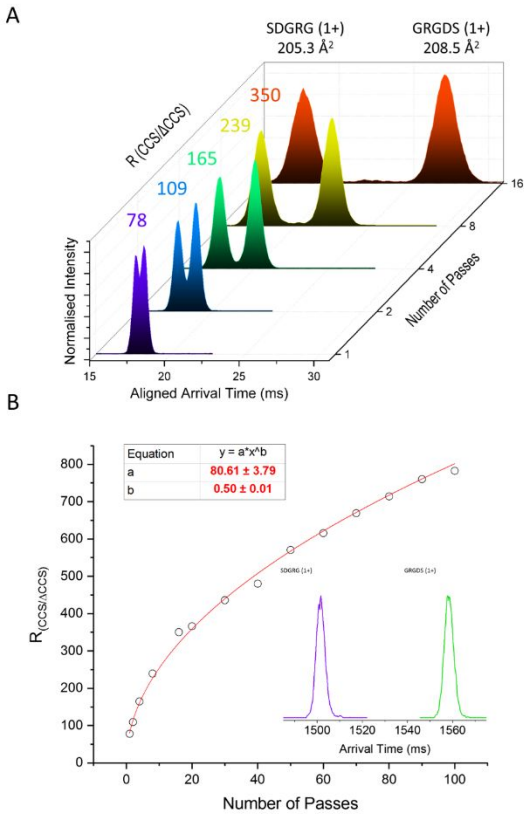


Figure 3. cIM resolution investigation of the reverse sequence peptides SDGRG and GRGDS, $[M+H]^+$ (*m/z* 491.2). A: ATDs of the two peptides vs passes around the cIM. The ATD peak tops for SDGRG have been aligned with that of the single pass for comparison. B: *R* (*CCS*/Δ*CCS*) vs passes around the cIM. Circles represent the experimentally measured values; the red line corresponds to the fitted curve. The ATDs obtained after 100 passes around the device are inset. TW: 30 V.

used to individually select the mobility peaks after 15 passes for further passes around the cIM. Figure 3B shows a plot of the mobility resolution as a function of number of passes, to a maximum of 100 (98 m). At 100 passes *R* is indicated to be around 750, the individual mobility peaks at this value are shown inset in Figure 3B. Fitting a power law function ($y=ax^b$) to these data show that the mobility resolution increases as the square root (b=0.5) of the number of passes, as expected from theory (Eq. 1). The derived *R*, coefficient 'a' (~81), is essentially the same as that obtained directly from the single pass measurement (78).

**Transmission:** An important requirement of the cIM is that, in operation, high ion transmission is maintained to facilitate analyses at levels close to or at the limits of detection of the base Q-ToF mass spectrometer. The implementation here of ion accumulation in the trap region during the previous mobility separation (as on a standard SYNAPT) provides close to 100% duty cycle. So, to investigate the effect of cIM operation on transmission, the signal of the GRGDS peptide was investigated as a function of number of passes. The sample was infused into the ESI source and the ion at *m/z* 491.2 $[M+H]^+$ selected using the quadrupole. Figure 4 shows the peak area (transmission) of the *m/z* 491.2 ATD for 0 to 100 passes around the cIM. It can be seen that the transmission drops by ~2.4% per pass at a TW height of 38 V, indicating minimal losses in the cIM. It should be noted that this is a typical value, obtained for a small, relatively robust ion. Species of widely different *m/z* or more labile species can, inevitably, undergo additional losses during the separation process.

**CCS Determination:** The motion of ions through a TWIM device is complex and, unlike classical drift tubes with uniform electric fields, CCS values cannot be determined from first principles. Consequently, TWIM devices have been successfully calibrated using species of known CCS value to allow CCS determination.[59–61] In this respect, the cIM device is no different and calibration data are shown in Figure S12 for a single pass where the CCS value determined is in good agreement with literature value. It should be noted that the uncertainties associated with the available literature CCS values, typically determined with linear field drift tube instrumentation (and used for TWIM calibration), are generally between 0.5-2%.[62] Consequently, determining higher accuracy CCS values using multiple passes around the cIM is limited until higher accuracy CCS standards can be generated.

**Multi-function experiments:** The multi-function capability of the cIM has been investigated using the three pentasaccharides and ubiquitin. Mobility resolution values stated below are calculated using a conservative $70\sqrt{n}$ form, where n is the number of passes around the cIM device.

*(i) IM Isolation and IMS2 – pentasaccharides*: Analysis of oligosaccharide sequence is often difficult with the current MS and single-stage IM-MS technology. Not only are the precursor ions often isomeric, they also produce isomeric fragments.[63] Three such pentasaccharides were infused as a mixture into the ESI source of the instrument and the ATD of the $[M+Na]^+$ species at *m/z* 851.3 (quadrupole-selected) recorded. After 3 passes around the cIM (*R* ~120), the three pentasaccharides can be easily distinguished in the ATD, see Figure 5A. The number of cIM passes was increased to 7 (*R* ~ 185) at which point the lowest mobility ion species (branched mannopentaose) was about to be overtaken (due to wrap-around) by the highest mobility ion species (cellopentaose) and additional peaks have become visible in the ATD (Figure 5B, Figure S10). These data are in good agreement with the observations made by Deng *et al.*[64] on their high-resolution SLIM system. To investigate the two central peaks associated with the maltopentaose in more detail, the '*IM isolation*' control sequence was set up to eject and remove the ion species related to the other two pentasaccharides (Figure 5B), allowing further separation of the remaining ions. Figure 5C shows the separation achieved after a further 14 passes (21 passes total, *R*~320) with the peaks nearly baseline resolved and not showing any additional fine structure.

Further investigation of the two peaks in Figure 5C is now possible. In turn, the mobility selected components were ejected to the pre-array store then re-injected to the cIM with increased energy resulting in collision induced dissociation (CID). The resulting product ion mass spectra, shown in Figures 5E and 5F, are essentially identical. The product ions were then mobility separated for 6 passes ($R$~170), after which comparison of product ion ATDs from the two precursors indicated some differences, see Figure 5D. For example, the *m/z* 689.2 product ions have ATDs which reflect the precursor mobility difference, implying that the structural difference has been retained, whereas the *m/z* 671.2 ion ATDs are identical, implying that the structural difference has been lost in this product ion. A more detailed investigation of these pentasaccharide species is reported in a recent publication by Ujma *et al*.[65]

*(ii) IM Isolation and IMS³ – Ubiquitin*: Conformations of gaseous protein ions are the subject of intense study and the use of multidimensional IMS experiments for such analyses was pioneered by the Clemmer group.[19,52,66] Here, we illustrate analogous experiments performed on the cIM platform. The ubiquitin sample was infused into the ESI source and the 6+ charge state (*m/z* 1428) selected using the quadrupole. A variety of IMS experiments were then performed using the cIM device (see Figure 6). Initially, the '*IM isolation*' functionality was used to isolate a narrow section (2 ms) of the protein ATD after the first pass (black ATD). The selected section continues on for a second pass (red ATD) while the unwanted ions are '*ejected-to-ToF*'. The ATDs of the selected ions were then sequentially recorded up to 6 passes (grey ATDs). Unlike the three pentasaccharides (Figure 5), increasing the number of passes does not reveal 'new' components, instead the ATDs appear broader and asymmetric. According to theory, the diffusion-limited ATD of 6+ ions existing in a single conformation would be expected to be √6 times narrower than that of singly charged ions (instrument $R \sim 70\sqrt{n}.\sqrt{6}$) . This is certainly not the case here (see Fig. S13) and can be potentially rationalized two ways: firstly, many closely related but dynamically isolated and stable conformations could be present.[35] It is important to remember that the ATDs presented here represent the summation of several thousand ion counts. In principle *every* detected ubiquitin ion could have a *unique* conformation and subsequent arrival time. Because of this inherent heterogeneity, it may not be possible to both resolve and detect all the different ubiquitin ions; secondly, conformer interconversion could be occurring on the time-scale of the IM experiment, effectively 'blurring' the separation.[8] This can be readily investigated using the cIM functionality and is presented in Figure 6 (IMS², IMS³). After the 6 passes around the cIM, *all* the IM isolated ions (i.e. the grey ATD between 100 and 120 ms) were ejected to the pre-array store, re-injected under non-activating conditions and subjected to 1 pass around the cIM (n+1 pass, purple ATD, +0V in Figure 6). Comparison of this ATD with that obtained after 2 passes (red) indicates that some conformer interconversion has occurred in that a lower mobility component is now present (indicated by an asterisk). Interestingly, the 'new' component resembles that observed (but not IM isolated) in the initial 1 pass (black) ATD. In order to further investigate possible conformer interconversion, the ubiquitin ions were re-injected into the array using higher voltage offsets (purple ATDs). Upon activation, a plethora of components with lower mobility appear, suggesting extension (unfolding) of the protein structure.[67] Importantly, the extent of

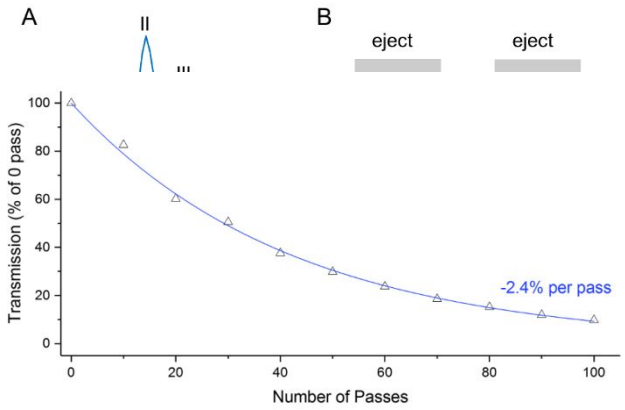


Figure 4. Transmission vs passes around the cIM , investigated using GRGDS, $[M+H]^+$ ( *m/z* 491.2). TW: 38 V

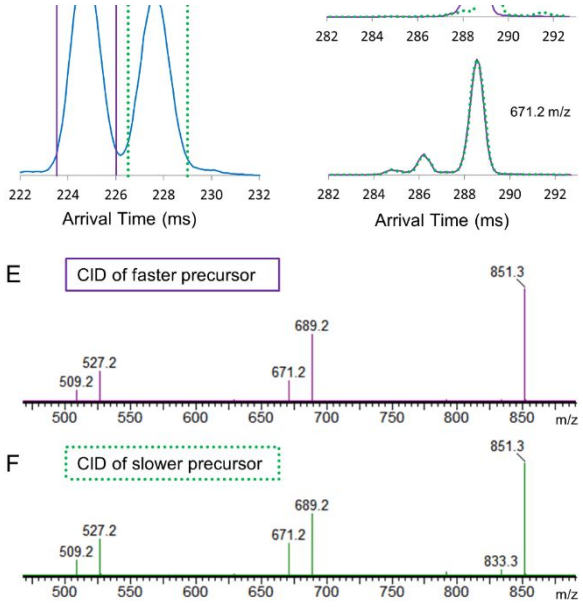


Figure 5. Multi-function IM analysis of isomeric pentasaccharides. A: ATD of (I) cellopentaose, (II) maltopentaose and (III) branched mannopentaose after three passes around the cIM. B: ATD after 7 passes. The control sequence is next set up to selectively eject species I and III (grey boxes). C: ATD of maltopentaose after 21 passes. Colored sections correspond to populations selectively ejected to the store and subjected to CID (200 eV) on re-injection. D: ATDs of product ions (*m/z* 689.2 and 671.2) originating from the two cIM separated precursors. E, F: corresponding mass spectra of the CID products. TW: 45 V.

interconversion/unfolding induced by subjecting the protein ions to 6 passes around cIM, ejection and re-injection appears minimal compared to unfolding induced by purposeful activation. Multi-stage IMS allows further studies of unfolding. As an example of IMS³, a subset of the activated ubiquitin ions (purple ATD, +30V, green arrow) was ejected to the pre-array store and re-injected at increased voltage offsets (green ATDs). Interestingly, the +40V activation of the subset of pre-activated ions results in some compaction of the protein structure. Then, at +60V offset, extended populations dominate and the ATD is superimposable with that obtained in the previous experiment (purple ATD, +60V). Collectively, these data suggest that on progression to fully extended states, a significant proportion of the selected (partially unfolded) ubiquitin 6+ ions can convert to more compact, intermediate form(s) before undergoing

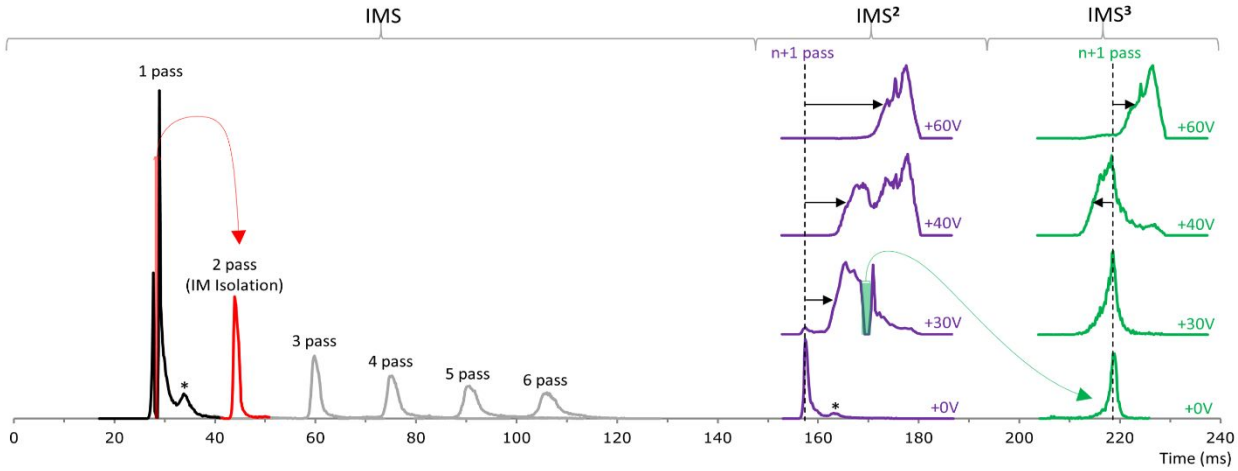


Figure 6. IM isolation and IMS$^n$ capabilities of the instrument demonstrated with ubiquitin 6+ ions. After the first pass (black ATD), a 2 ms wide section of the ATD is allowed to proceed to the 2$^{nd}$ pass (red arrow, red ATD) while the rest of the ions are removed (IM isolation). The selected ions are then subjected to further passes around the cIM (grey ATDs). After 6 passes, the ions are ejected to the store, re-injected and subjected to one pass cIM separation (purple ATD, +0V). The stacked plots are with increasing re-injection voltage (purple ATDs), for activation (IMS$^2$). Then, a subset of activated population (+30V, purple ATD) is ejected to the store, re-injected and subjected to one pass around the cIM (green arrow, green ATD). Again, the selected ions are activated using increasing injection voltage (IMS$^3$, stacked green ATDs). TW: 35 V.

extension. Also, that all the extended forms can be generated from the selected, pre-activated subset of ions.

The above phenomena as well as the effect of prolonged exposure of protein ions to the gas phase environment are the subject of a recent study using the cIM.[68]

## CONCLUSIONS AND OUTLOOK

The design and performance of a TW-enabled multi-pass, cyclic ion mobility separator, incorporated in a Q-cIM-ToF geometry, has been described. The 'dial-up' mobility resolution and multi-function capability (including IMS$^n$) are the key features of the cIM and represent a notable step forward in flexibility and utility of IM separators. The majority of the functionality presented here is enabled by a, multi-function, array of TW-enabled electrodes which allow control of ion entry and exit to the cIM as well as ion separation. The development of flexible instrument control software allows multi-function experiments to be performed through configuration of function sequences, enabling a wide range of complex IM based experiments.

The resolution of the 98 cm path-length cIM has been shown to increase with the square root of the number of passes around the device with a single pass *R* of ~80 and a 100 pass *R* of around 750. The multi-function capability has been highlighted using the separation of three, isomeric, pentasaccharide species and the 6+ ion of ubiquitin. Such experiments hint at the potential of this approach for in-depth structural evaluation of isomeric species, which is hard to achieve by any other means.

It has been shown that the cIM can generate CCS values for a single pass via calibration, in the same manner as existing linear TWIM devices. The accuracy of available CCS standards currently limits the accuracy of measurements that can be obtained using the cIM. Consequently, a wider discussion regarding the generation and use of CCS in higher resolution IM separations will be required.

## ASSOCIATED CONTENT

### Supporting Information

Figures highlighting SIMION electrode geometries, cIM charge capacity, ion spatial distributions, mobility resolution simulations, cIM photographs, array schematic, potential energy diagrams, functional cIM operation, control software GUI, wrap-around illustration, ToF resolution, CCS calibration, ubiquitin ATD comparison.

## AUTHOR INFORMATION

### Corresponding Author

*e-mail: kevin_giles@waters.com

### Author Contributions

The manuscript was written through contributions of all authors.

## ACKNOWLEDGMENT

The authors would like to acknowledge the skill and technical expertise of the engineering team: Peter Carney, John Garside, Bharat Chande, Peter Nixon, Praveen Harapanahalli, James Harrison, Darren Hewitt, John Iveson, Witold Niklewski, Sandra Richardson, Graham Scambler, Chris Wheeldon and many others at Waters Wilmslow.

## REFERENCES

(1) Eiceman, G. A.; Karpas, Z.; Hill, H. H. *Ion Mobility Spectrometry*; CRC Press: Boca Raton, 2013.

(2) Mason, E. A.; McDaniel, E. W. *Transport Properties of Ions in Gases*; John Wiley & Sons, Ltd, 1988.

(3) Kanu, A. B.; Dwivedi, P.; Tam, M.; Matz, L.; Hill, H. H. Ion Mobility-Mass Spectrometry. *J. Mass Spectrom.* **2008**, *43* (1), 1–22.

(4) May, J. C.; McLean, J. A. Ion Mobility-Mass Spectrometry: Time-Dispersive Instrumentation. *Anal. Chem.* **2015**, *87* (3), 1422–1436.

(5) Kemper, P. R.; Bowers, M. T. A Hybrid Double-Focusing Mass Spectrometer—High-Pressure Drift Reaction Cell to Study Thermal Energy Reactions of Mass-Selected Ions. *J. Am. Soc. Mass Spectrom.* **1990**, *1* (3), 197–207.

(6) Jarrold, M. F.; Honea, E. C. Dissociation of Large Silicon Clusters: The Approach to Bulk Behavior. *J. Phys. Chem.* **1991**, *95* (23), 9181–9185.

(7) Wittmer, Doug.; Chen, Y. Hong.; Luckenbill, B. K.; Hill, H. H. Electrospray Ionization Ion Mobility Spectrometry. *Anal. Chem.* **1994**, *66* (14), 2348–2355.

(8) Clemmer, D. E.; Hudgins, R. R.; Jarrold, M. F. Naked Protein Conformations: Cytochrome c in the Gas Phase. *J. Am. Chem. Soc.* **1995**, *117* (40), 10141–10142.

(9) Wu, C.; Siems, W. F.; Asbury, G. R.; Hill, H. H. Electrospray Ionization High-Resolution Ion Mobility Spectrometry−Mass Spectrometry. *Anal. Chem.* **1998**, *70* (23), 4929–4938.

(10) Hoaglund, C. S.; Valentine, S. J.; Sporleder, C. R.; Reilly, J. P.; Clemmer, D. E. Three-Dimensional Ion Mobility/TOFMS Analysis of Electrosprayed Biomolecules. *Anal. Chem.* **1998**, *70* (11), 2236–2242.

(11) Wyttenbach, T.; Kemper, P. R.; Bowers, M. T. Design of a New Electrospray Ion Mobility Mass Spectrometer. *Int. J. Mass Spectrom.* **2001**, *212* (1–3), 13–23.

(12) Valentine, S. J.; Koeniger, S. L.; Clemmer, D. E. A Split-Field Drift Tube for Separation and Efficient Fragmentation of Biomolecular Ions. *Anal. Chem.* **2003**, *75* (22), 6202–6208.

(13) Gerlich, D. Inhomogeneous RF Fields: A Versatile Tool for the Study of Processes with Slow Ions. In *Advances in Chemical Physics*; John Wiley & Sons, Ltd, 1992; pp 1–176.

(14) Hoaglund, C. S.; Valentine, S. J.; Clemmer, D. E. An Ion Trap Interface for ESI−Ion Mobility Experiments. *Anal. Chem.* **1997**, *69* (20), 4156–4161.

(15) Shaffer, S. A.; Prior, D. C.; Anderson, G. A.; Udseth, H. R.; Smith, R. D. An Ion Funnel Interface for Improved Ion Focusing and Sensitivity Using Electrospray Ionization Mass Spectrometry. *Anal. Chem.* **1998**, *70* (19), 4111–4119.

(16) Giles, K.; Pringle, S. D.; Worthington, K. R.; Little, D.; Wildgoose, J. L.; Bateman, R. H. Applications of a Travelling Wave-Based Radio-Frequency-Only Stacked Ring Ion Guide. *Rapid Commun. Mass Spectrom.* **2004**, *18* (20), 2401–2414.

(17) Thalassinos, K.; Slade, S. E.; Jennings, K. R.; Scrivens, J. H.; Giles, K.; Wildgoose, J.; Hoyes, J.; Bateman, R. H.; Bowers, M. T. Ion Mobility Mass Spectrometry of Proteins in a Modified Commercial Mass Spectrometer. *Int. J. Mass Spectrom.* **2004**, *236* (1–3), 55–63.

(18) Tang, K.; Shvartsburg, A. A.; Lee, H.-N.; Prior, D. C.; Buschbach, M. A.; Li, F.; Tolmachev, A. V.; Anderson, G. A.; Smith, R. D. High-Sensitivity Ion Mobility Spectrometry/Mass Spectrometry Using Electrodynamic Ion Funnel Interfaces. *Anal. Chem.* **2005**, *77* (10), 3330–3339.

(19) Merenbloom, S. I.; Koeniger, S. L.; Valentine, S. J.; Plasencia, M. D.; Clemmer, D. E. IMS−IMS and IMS−IMS−IMS/MS for Separating Peptide and Protein Fragment Ions. *Anal. Chem.* **2006**, *78* (8), 2802–2809.

(20) Giles, K.; Pringle, S.; Wildgoose, J.; Bateman, R. Characterising A Travelling Wave-Based Ion Mobility Separator. In *Annual Conference Proceedings*; ASMS: Seattle, 2006.

(21) Pringle, S. D.; Giles, K.; Wildgoose, J. L.; Williams, J. P.; Slade, S. E.; Thalassinos, K.; Bateman, R. H.; Bowers, M. T.; Scrivens, J. H. An Investigation of the Mobility Separation of Some Peptide and Protein Ions Using a New Hybrid Quadrupole/Travelling Wave IMS/Oa-ToF Instrument. *Int. J. Mass Spectrom.* **2007**, *261* (1), 1–12.

(22) Ridgeway, M. E.; Lubeck, M.; Jordens, J.; Mann, M.; Park, M. A. Trapped Ion Mobility Spectrometry: A Short Review. *Int. J. Mass Spectrom.* **2018**, *425*, 22–35.

(23) May, J. C.; Dodds, J. N.; Kurulugama, R. T.; Stafford, G. C.; Fjeldsted, J. C.; McLean, J. A. Broadscale Resolving Power Performance of a High Precision Uniform Field Ion Mobility-Mass Spectrometer. *The Analyst* **2015**, *140* (20), 6824–6833.

(24) McLean, J. A.; Ruotolo, B. T.; Gillig, K. J.; Russell, D. H. Ion Mobility–Mass Spectrometry: A New Paradigm for Proteomics. *Int. J. Mass Spectrom.* **2005**, *240* (3), 301–315.

(25) Bohrer, B. C.; Merenbloom, S. I.; Koeniger, S. L.; Hilderbrand, A. E.; Clemmer, D. E. Biomolecule Analysis by Ion Mobility Spectrometry. *Annu. Rev. Anal. Chem.* **2008**, *1* (1), 293–327.

(26) Jurneczko, E.; Barran, P. E. How Useful Is Ion Mobility Mass Spectrometry for Structural Biology? The Relationship between Protein Crystal Structures and Their Collision Cross Sections in the Gas Phase. *The Analyst* **2011**, *136* (1), 20–28.

(27) Fasciotti, M.; Lalli, P. M.; Klitzke, C. F.; Corilo, Y. E.; Pudenzi, M. A.; Pereira, R. C. L.; Bastos, W.; Daroda, R. J.; Eberlin, M. N. Petroleomics by Traveling Wave Ion Mobility–Mass Spectrometry Using CO2 as a Drift Gas. *Energy Fuels* **2013**, *27* (12), 7277–7286.

(28) Ben-Nissan, G.; Sharon, M. The Application of Ion-Mobility Mass Spectrometry for Structure/Function Investigation of Protein Complexes. *Curr. Opin. Chem. Biol.* **2018**, *42*, 25–33.

(29) Donald, A. W.; Prell, J. S. *Advances in Ion Mobility-Mass Spectrometry: Fundamentals, Instrumentation and Applications*, 1st ed.; Elsevier, 2019; Vol. 83.

(30) Ibrahim, Y. M.; Baker, E. S.; Danielson, W. F.; Norheim, R. V.; Prior, D. C.; Anderson, G. A.; Belov, M. E.; Smith, R. D. Development of a New Ion Mobility Time-of-Flight Mass Spectrometer. *Int. J. Mass Spectrom.* **2015**, *377*, 655–662.

(31) Stow, S. M.; Causon, T. J.; Zheng, X.; Kurulugama, R. T.; Mairinger, T.; May, J. C.; Rennie, E. E.; Baker, E. S.; Smith, R. D.; McLean, J. A.; et al. An Interlaboratory Evaluation of Drift Tube Ion Mobility–Mass Spectrometry Collision Cross Section Measurements. *Anal. Chem.* **2017**, *89* (17), 9048–9055.

(32) Giles, K.; Palmer, M.; Richardson, K.; Tomczyk, N. Comparison Of CCS(N2) Measurements Obtained From Two Different T-Wave IMS Systems With Direct Measurements Using A Drift Tube IMS. In *Annual Conference Proceedings*; ASMS: St Louis, 2015.

(33) Shvartsburg, A. A.; Smith, R. D. Fundamentals of Traveling Wave Ion Mobility Spectrometry. *Anal. Chem.* **2008**, *80* (24), 9689–9699.

(34) Moseley, J. T.; Gatland, I. R.; Martin, D. W.; McDaniel, E. W. Measurement of Transport Properties of Ions in Gases; Results for K + Ions in N 2. *Phys. Rev.* **1969**, *178* (1), 234–239.

(35) Koeniger, S. L.; Merenbloom, S. I.; Clemmer, D. E. Evidence for Many Resolvable Structures within Conformation Types of Electrosprayed Ubiquitin Ions. *J. Phys. Chem. B* **2006**, *110* (13), 7017–7021.

(36) Kemper, P. R.; Dupuis, N. F.; Bowers, M. T. A New, Higher Resolution, Ion Mobility Mass Spectrometer. *Int. J. Mass Spectrom.* **2009**, *287* (1), 46–57.

(37) Dugourd, Ph.; Hudgins, R. R.; Clemmer, D. E.; Jarrold, M. F. High-Resolution Ion Mobility Measurements. *Rev. Sci. Instrum.* **1997**, *68* (2), 1122–1129.

(38) Kirk, A. T.; Allers, M.; Cochems, P.; Langejuergen, J.; Zimmermann, S. A Compact High Resolution Ion Mobility Spectrometer for Fast Trace Gas Analysis. *Analyst* **2013**, *138* (18), 5200–5207.

(39) May, J. C.; Russell, D. H. A Mass-Selective Variable-Temperature Drift Tube Ion Mobility-Mass Spectrometer for Temperature Dependent Ion Mobility Studies. *J. Am. Soc. Mass Spectrom.* **2011**, *22* (7), 1134–1145.

(40) Ujma, J.; Giles, K.; Morris, M.; Barran, P. E. New High Resolution Ion Mobility Mass Spectrometer Capable of Measurements of Collision Cross Sections from 150 to 520 K. *Anal. Chem.* **2016**, *88* (19), 9469–9478.

(41) Merenbloom, S. I.; Glaskin, R. S.; Henson, Z. B.; Clemmer, D. E. High-Resolution Ion Cyclotron Mobility Spectrometry. *Anal. Chem.* **2009**, *81* (4), 1482–1487.

(42) Glaskin, R. S.; Ewing, M. A.; Clemmer, D. E. Ion Trapping for Ion Mobility Spectrometry Measurements in a Cyclical Drift Tube. *Anal. Chem.* **2013**, *85* (15), 7003–7008.

(43) Bateman, R. H.; Giles, K.; Pringle, Steven D.; Wildgoose, J. L. Closed Loop Ion Guide with Pseudo-Potential Well. US9281172B2, 2005.

(44) Giles, K.; Wildgoose, J.; Pringle, S.; Garside, J.; Carney, P.; Nixon, P.; Langridge, D. Design and Utility of a Multi-Pass

Cyclic Ion Mobility Separator. In *Annual Conference Proceedings*; ASMS: Baltimore, 2014.

(45) Giles, K.; Wildgoose, J.; Pringle, S.; Langridge, D.; Nixon, P.; Garside, J.; Carney, P. Characterising a T-Wave Enabled Multi-Pass Cyclic Ion Mobility Separator. In *Annual Conference Proceedings*; ASMS: St Louis, 2015.

(46) Ibrahim, Y. M.; Hamid, A. M.; Deng, L.; Garimella, S. V. B.; Webb, I. K.; Baker, E. S.; Smith, R. D. New Frontiers for Mass Spectrometry Based upon Structures for Lossless Ion Manipulations. *Analyst* **2017**, *142* (7), 1010–1021.

(47) Deng, L.; Webb, I. K.; Garimella, S. V. B.; Hamid, A. M.; Zheng, X.; Norheim, R. V.; Prost, S. A.; Anderson, G. A.; Sandoval, J. A.; Baker, E. S.; et al. Serpentine Ultralong Path with Extended Routing (SUPER) High Resolution Traveling Wave Ion Mobility-MS Using Structures for Lossless Ion Manipulations. *Anal. Chem.* **2017**, *89* (8), 4628–4634.

(48) Loboda, A. Novel Ion Mobility Setup Combined with Collision Cell and Time-of-Flight Mass Spectrometer. *J. Am. Soc. Mass Spectrom.* **2006**, *17* (5), 691–699.

(49) Fernandez-Lima, F. A.; Kaplan, D. A.; Park, M. A. Integration of Trapped Ion Mobility Spectrometry with Mass Spectrometry. *Rev. Sci. Instrum.* **2011**, *82* (12), 126106.

(50) Adams, K. J.; Montero, D.; Aga, D.; Fernandez-Lima, F. Isomer Separation of Polybrominated Diphenyl Ether Metabolites Using NanoESI-TIMS-MS. *Int. J. Ion Mobil. Spectrom.* **2016**, *19* (2), 69–76.

(51) Jeanne Dit Fouque, K.; Ramirez, C. E.; Lewis, R. L.; Koelmel, J. P.; Garrett, T. J.; Yost, R. A.; Fernandez-Lima, F. Effective Liquid Chromatography–Trapped Ion Mobility Spectrometry–Mass Spectrometry Separation of Isomeric Lipid Species. *Anal. Chem.* **2019**, *91* (8), 5021–5027.

(52) Koeniger, S. L.; Merenbloom, S. I.; Valentine, S. J.; Jarrold, M. F.; Udseth, H. R.; Smith, R. D.; Clemmer, D. E. An IMS−IMS Analogue of MS−MS. *Anal. Chem.* **2006**, *78* (12), 4161–4174.

(53) Li, H.; Bendiak, B.; Siems, W. F.; Gang, D. R.; Hill, H. H. Carbohydrate Structure Characterization by Tandem Ion Mobility Mass Spectrometry (IMMS)2. *Anal. Chem.* **2013**, *85* (5), 2760–2769.

(54) Liu, F. C.; Ridgeway, M. E.; Park, M. A.; Bleiholder, C. Tandem Trapped Ion Mobility Spectrometry. *Analyst* **2018**, *143* (10), 2249–2258.

(55) Giles, K.; Ujma, J.; Green, M.; Richardson, K.; Langridge, D.; Tomczyk, N. Design and Performance of a Second-Generation Cyclic Ion Mobility Enabled Q-ToF. In *Annual Conference Proceedings*; ASMS: Indianapolis, 2017.

(56) Ujma, J.; Richardson, S.; Giles, K. A Multi-Function Cyclic Ion Mobility – Mass Spectrometry System. In *Annual Conference Proceedings*; ASMS: San Diego, 2018.

(57) Richardson, K.; Langridge, D.; Giles, K. Fundamentals of Travelling Wave Ion Mobility Revisited: I. Smoothly Moving Waves. *Int. J. Mass Spectrom.* **2018**, *428*, 71–80.

(58) Giles, K.; Williams, J. P.; Campuzano, I. Enhancements in Travelling Wave Ion Mobility Resolution. *Rapid Commun. Mass Spectrom.* **2011**, *25* (11), 1559–1566.

(59) Ruotolo, B. T.; Benesch, J. L. P.; Sandercock, A. M.; Hyung, S.-J.; Robinson, C. V. Ion Mobility–Mass Spectrometry Analysis of Large Protein Complexes. *Nat. Protoc.* **2008**, *3* (7), 1139–1152.

(60) Thalassinos, K.; Grabenauer, M.; Slade, S. E.; Hilton, G. R.; Bowers, M. T.; Scrivens, J. H. Characterization of Phosphorylated Peptides Using Traveling Wave-Based and Drift Cell Ion Mobility Mass Spectrometry. *Anal. Chem.* **2009**, *81* (1), 248–254.

(61) Bush, M. F.; Hall, Z.; Giles, K.; Hoyes, J.; Robinson, C. V.; Ruotolo, B. T. Collision Cross Sections of Proteins and Their Complexes: A Calibration Framework and Database for Gas-Phase Structural Biology. *Anal. Chem.* **2010**, *82* (22), 9557–9565.

(62) May, J. C.; Goodwin, C. R.; Lareau, N. M.; Leaptrot, K. L.; Morris, C. B.; Kurulugama, R. T.; Mordehai, A.; Klein, C.; Barry, W.; Darland, E.; et al. Conformational Ordering of Biomolecules in the Gas Phase: Nitrogen Collision Cross Sections Measured on a Prototype High Resolution Drift Tube Ion Mobility-Mass Spectrometer. *Anal. Chem.* **2014**, *86* (4), 2107–2116.

(63) Gaye, M. M.; Kurulugama, R.; Clemmer, D. E. Investigating Carbohydrate Isomers by IMS-CID-IMS-MS: Precursor and Fragment Ion Cross-Sections. *Analyst* **2015**, *140* (20), 6922–6932.

(64) Deng, L.; Ibrahim, Y. M.; Baker, E. S.; Aly, N. A.; Hamid, A. M.; Zhang, X.; Zheng, X.; Garimella, S. V. B.; Webb, I. K.; Prost, S. A.; et al. Ion Mobility Separations of Isomers Based upon Long Path Length Structures for Lossless Ion Manipulations Combined with Mass Spectrometry. *ChemistrySelect* **2016**, *1* (10), 2396–2399.

(65) Ujma, Jakub; Ropartz, D.; Giles, K.; Richardson, Keith; Langridge, D.; Wildgoose, J.; Green, M.; Pringle, S. Cyclic Ion Mobility Mass Spectrometry Distinguishes Anomers and Open-Ring Forms of Pentasaccharides. *J. Am. Soc. Mass Spectrom.* **2019**, *30* (6), 1028–1037.

(66) Koeniger, S. L.; Clemmer, D. E. Resolution and Structural Transitions of Elongated States of Ubiquitin. *J. Am. Soc. Mass Spectrom.* **2007**, *18* (2), 322–331.

(67) Valentine, S. J.; Anderson, J. G.; Ellington, A. D.; Clemmer, D. E. Disulfide-Intact and -Reduced Lysozyme in the Gas Phase: Conformations and Pathways of Folding and Unfolding. *J. Phys. Chem. B* **1997**, *101* (19), 3891–3900.

(68) Eldrid, C.; Ujma, J.; Kalfas, S.; Tomczyk, Nicholas; Giles, K.; Morris, M.; Thalassinos, K. Gas Phase Stability of Protein Ions in a Cyclic Ion Mobility Spectrometry Travelling Wave Device. *Anal Chem* **2019**, *in press*. https://doi.org/10.1021/acs.analchem.8b05641

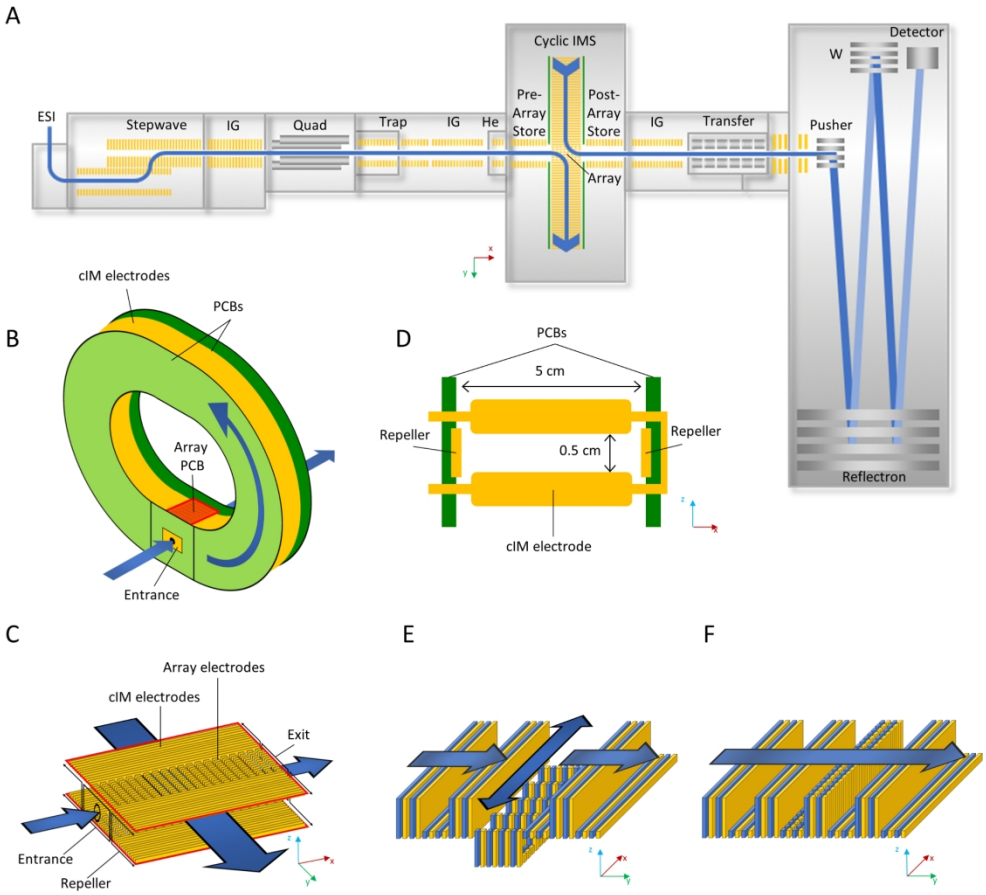


Figure 1. Instrument design. A: instrument overview (adapted in part with permission from ref 63. Copyright 2019, Ujma *et al*.) B: cIM device. C: ion entry/exit region, consisting of array electrodes. D: structure of cIM electrodes. E: Ion injection/ejection mode, array TWs are applied in the x-(or -x) direction. F: Separation mode, array TWs are applied in the y-direction.

177x163mm (286 x 286 DPI)

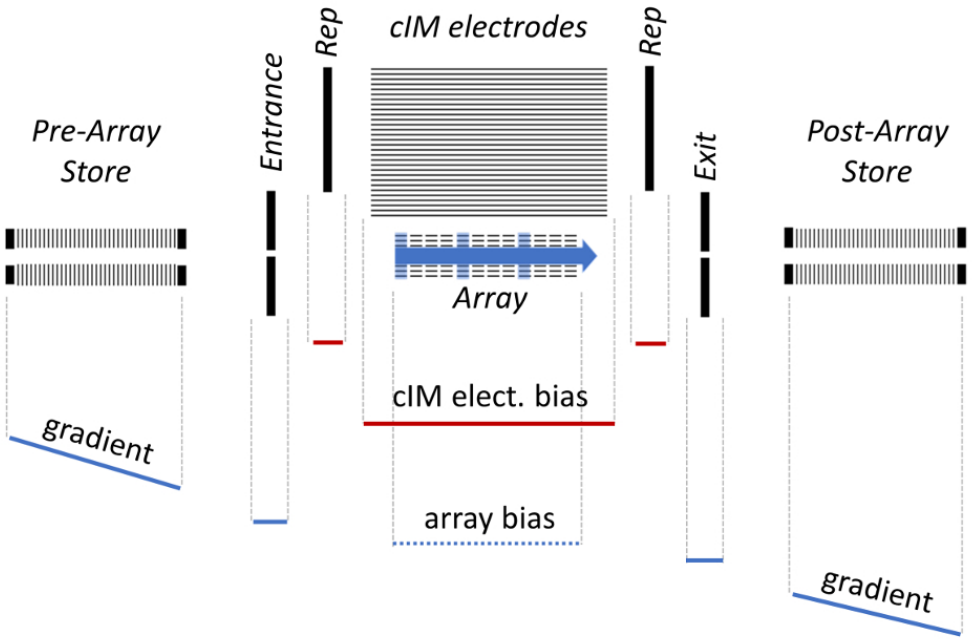


Figure 2. Potential energy schematic of the cIM region voltages during 'bypass' mode. Settings changeable on a 'per function' basis: blue lines. Settings changeable on 'per sequence' basis: red lines. Blue arrows indicate the array TW direction. Schematics of other functions are presented in the Figure S8.

84x56mm (286 x 286 DPI)

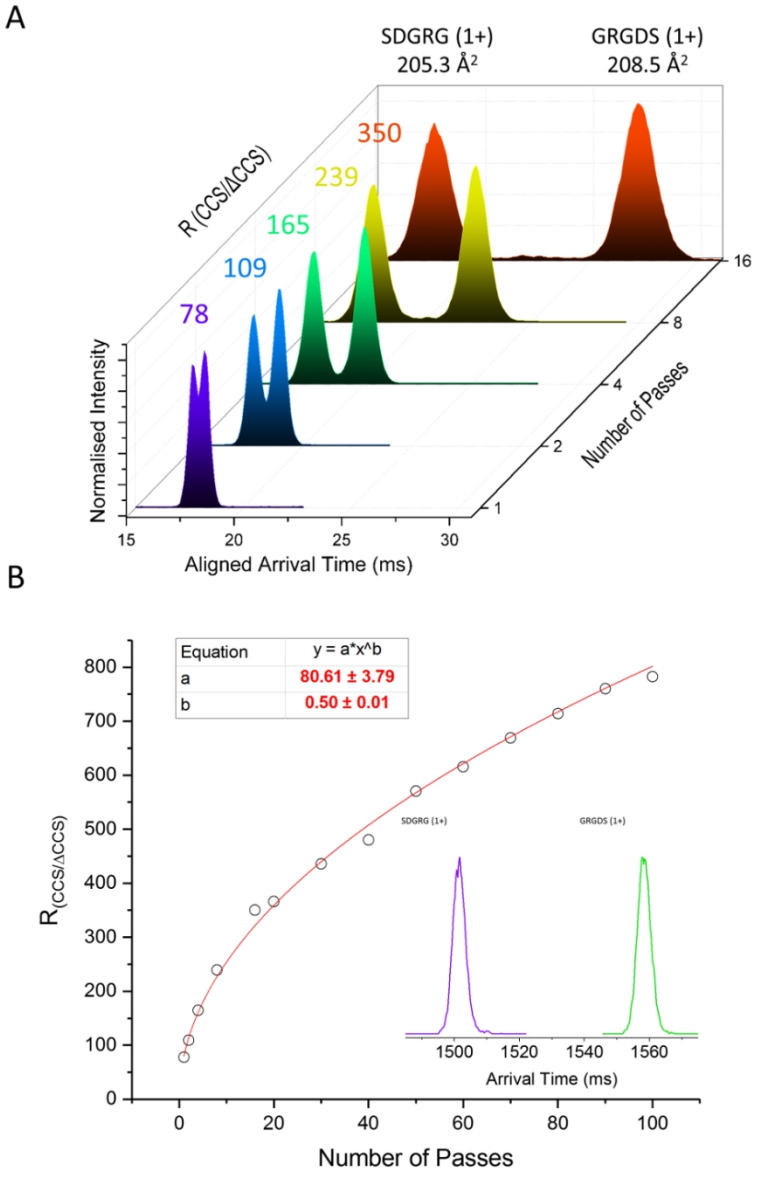


Figure 3. cIM resolution investigation of the reverse sequence peptides SDGRG and GRGDS, $[M+H]^+$ (*m/z* 491.2). A: ATDs of the two peptides vs passes around the cIM. The ATD peak tops for SDGRG have been aligned with that of the single pass for comparison. B: R (CCS/ΔCCS) vs passes around the cIM. Circles represent the experimentally measured values; the red line corresponds to the fitted curve. The ATDs obtained after 100 passes around the device are inset. TW: 30 V.

84x130mm (286 x 286 DPI)

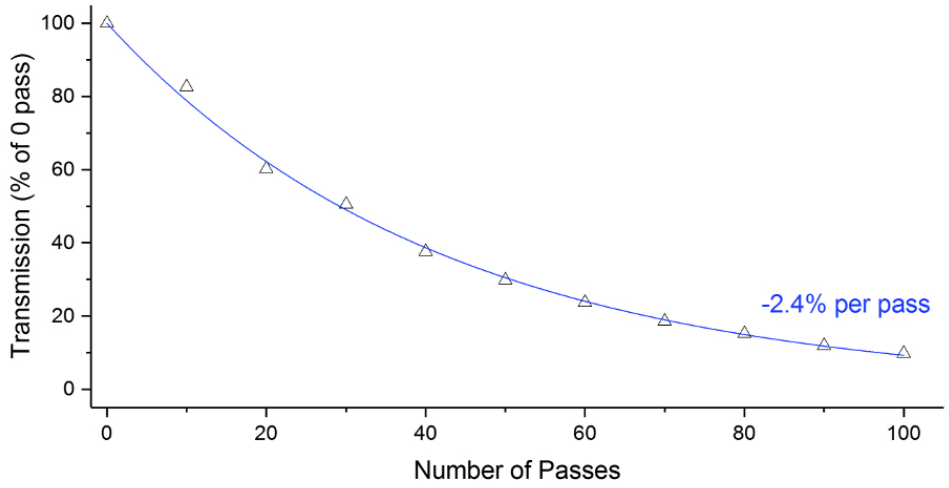


Figure 4. Transmission vs passes around the cIM, investigated using GRGDS, $[M+H]^+$ (*m/z* 491.2). TW: 38 V

84x44mm (286 x 286 DPI)

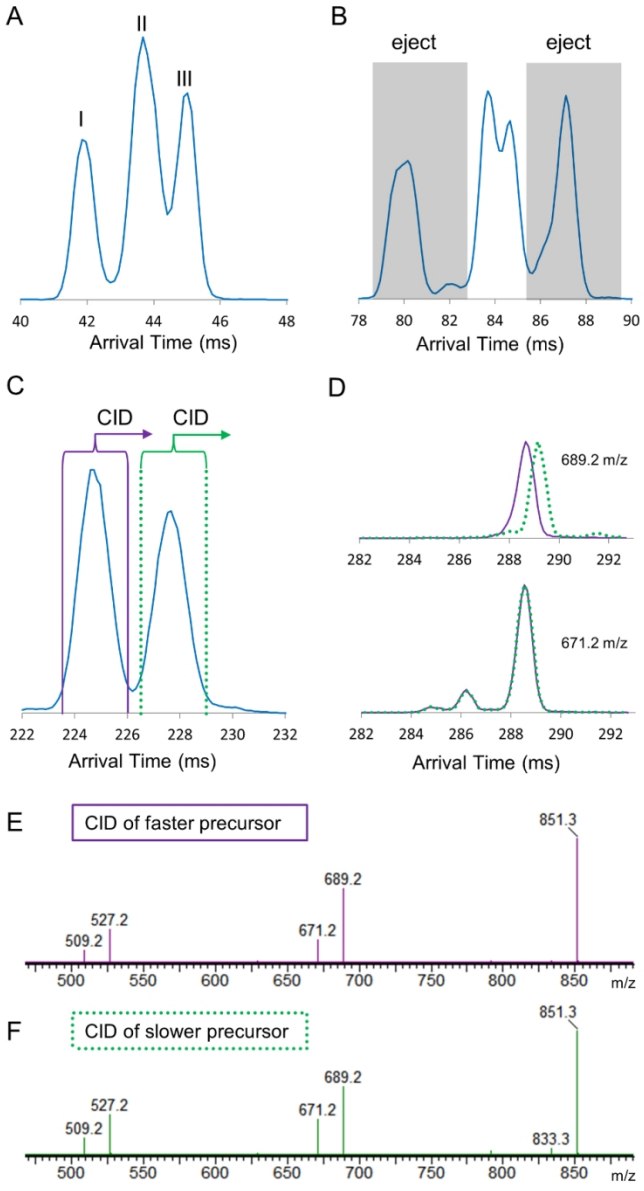


Figure 5. Multi-function IM analysis of isomeric pentasaccharides. A: ATD of (I) cellopentaose, (II) maltopentaose and (III) branched mannopentaose after three passes around the cIM. B: ATD after 7 passes. The control sequence is next set up to selectively eject species I and III (grey boxes). C: ATD of maltopentaose after 21 passes. Colored sections correspond to populations selectively ejected to the store and subjected to CID (200 eV) on re-injection. D: ATDs of product ions (m/z 689.2 and 671.2) originating from the two cIM separated precursors. E, F: corresponding mass spectra of the CID products. TW: 45 V.

84x153mm (286 x 286 DPI)

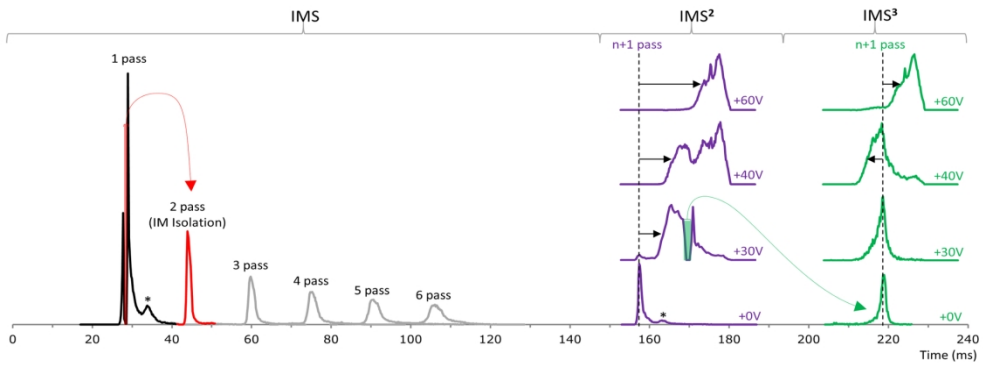


Figure 6. IM isolation and $IMS^n$ capabilities of the instrument demonstrated with ubiquitin 6+ ions. After the first pass (black ATD), a 2 ms wide section of the ATD is allowed to proceed to the 2nd pass (red arrow, red ATD) while the rest of the ions are removed (IM isolation). The selected ions are then subjected to further passes around the cIM (grey ATDs). After 6 passes, the ions are ejected to the store, re-injected and subjected to one pass cIM separation (purple ATD, +0V). The stacked plots are with increasing re-injection voltage (purple ATDs), for activation ($IMS^2$). Then, a subset of activated population (+30V, purple ATD) is ejected to the store, re-injected and subjected to one pass around the cIM (green arrow, green ATD). Again, the selected ions are activated using increasing injection voltage ($IMS^3$, stacked green ATDs). TW: 35 V.

177x65mm (300 x 300 DPI)

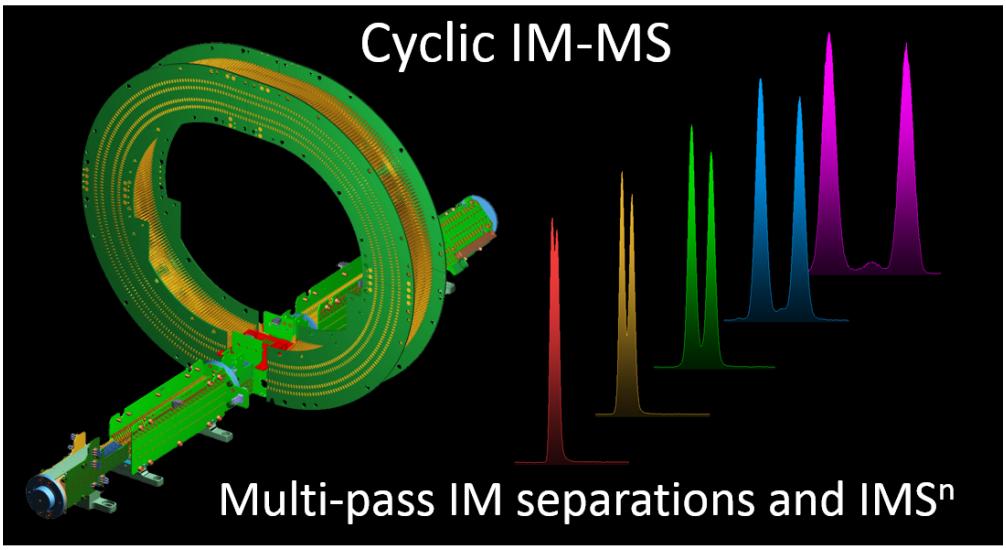
Cyclic IM-MS
Multi-pass IM separations and IMS$^n$